International Journal of Innovative Computing, Information and Control
Volume **11**, Number **1**, February **2015**
 ISSN 1349-4198
pp. 87–103

THE ESTIMATION OF GFR AND ERPF USING ADAPTIVE EDGE-BASED ACTIVE CONTOUR FOR THE SEGMENTATION OF STRUCTURES IN DYNAMIC RENAL SCINTIGRAPHY

Piyamas Suapang[1], Kobchai Dejhan[1] and Surapun Yimman[2]

[1]Department of Telecommunications Engineering
Faculty of Engineering
King Mongkut's Institute of Technology Ladkrabang
Bangkok 10520, Thailand
piyamas_suapang@yahoo.com; kdejhan@gmail.com

[2]Department of Industry Physics and Medical Instrument
Faculty of Applied Science
King Mongkut's University of Technology North Bangkok
Bangkok 10800, Thailand
sym4412@gmail.com

Received March 2014; revised July 2014

Abstract. *Dynamic renal scintigraphy is usually applied for the estimation of GFR and ERPF. The clearance of ^{99m}Tc-DTPA and ^{99m}Tc-MAG3 were the relatively index of GFR and ERPF in the clinical evaluation of patients with acute and chronic renal failure using camera-based methods. In camera-based methods it is necessary to manually delineate ROIs for ^{99m}Tc-DTPA and ^{99m}Tc-MAG3 calculation. The requirement may reduce the convenience and reliability of estimating GFR and ERPF from dynamic renal scintigraphy. This paper proposes the estimation of GFR and ERPF using adaptive edge-based active contour for the segmentation of structures in dynamic renal scintigraphy. The salient feature of proposed method is based on combining three other external force. First, the adaptive elastic parameter has been developed to automatically adjust the rigidity of the snake during its evolution towards an image contour. Second, the adaptive balloon force has been implemented to increase the GVF snake's captured range and convergence speed. Finally, a dynamic GVF force is introduced to provide an efficient evolution stop mechanism. Preliminary segmentation results demonstrate the potential of proposed method and are visually judged to be acceptable for clinical use in comparison with the original GVF snake method and manual segmentation by experts. Furthermore, the mean of estimating GFR and ERPF with the proposed method are successfully predicted and do not differ from APEX-XPERT program at the 5% level of significance.*
Keywords: Dynamic renal scintigraphy, Effective renal plasma flow, Glomerular filtration rate, Region of interest

1. **Introduction.** Measurement of absolute and relative renal function is a major role of dynamic renal scintigraphy. Figure 1 shows time-activity curves of a normal renal study. Regions of interest are set for both kidneys and the background. Counts in these regions are then digitally summed over each frame in the acquisition sequence to define the time-activity curve for each kidney. The clearance of ^{99m}Tc-diethylenetriamine-pentaacetic acid (^{99m}Tc-DTPA) and ^{99m}Tc-mercaptoacetyltriglycine (^{99m}Tc-MAG3) are a relatively new index of glomerular filtration rate (GFR) and effective renal plasma flow (ERPF), respectively. Camera-based methods without blood sampling have been described to calculate s^{99m}Tc-MAG3 clearance [1-7]. In the camera-based methods, it is necessary to select regions of interest (ROIs) for the kidneys and background areas, a task commonly

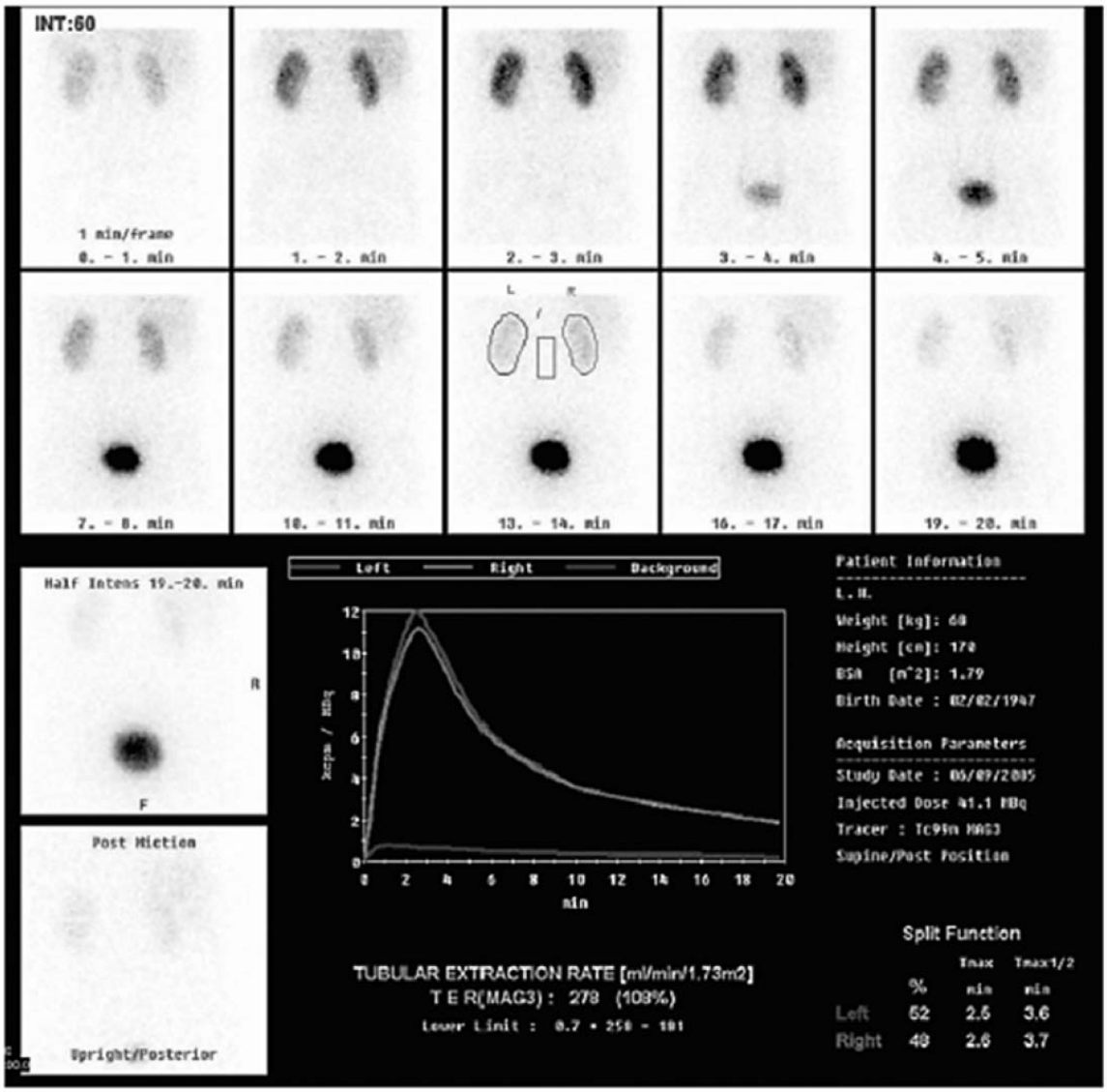

FIGURE 1. Time-activity curves of a normal renal study

performed by manual in an operator. Interoperator variability in drawing ROIs is a potential source of interoperator and interinstitutional difference in calculating indices of renal function [8-12]. Operator dependency can cause a substantial problem, especially in institutes with no physicians or technologists experienced in nuclear nephrology, and it may impair the feasibility and reliability of estimation of GFR and ERPF from dynamic renal scintigraphy.

Although several methods have been reported to decrease operator dependency in ROIs selection for the estimation of renal function [8-10,13-16], none has been widely accepted as a method of choice in clinical practice. In addition, accuracy in estimating GFR and ERPF with decreased operator dependency has not been addressed in previous reports. Because the purpose of ROIs selection in a camera-based methods is to quantitate GFR and ERPF, assessment of the accuracy of estimated renal function seems to be essential from determinable the success of defined ROIs. Furthermore, there has been a substantial amount of research on segmenting images with deformable models in recent years [17]. Notably active contours, known as "snakes", have been widely studied and applied in medical image analysis, and their applications include edge detection, segmentation of

objects, shape modeling and motion tracking [18,19]. Snakes were first introduced in 1987 by Kass et al. [20]. They generally represent an object boundary as a parameter curve or surface. An energy function is associated with the curve, so the problem of finding an object boundary is cast as an energy minimization process. Typically, the curves are affected by both an internal force and external force. A snake can locate object contours well, once an appropriate initialization is done. However, since the energy minimization is locally carried out, the located contours can be trapped by a local minimum. A number of methods have been proposed to improve the snake's performance [21,22]. Recently, Xu and Prince have proposed a new deformable model called the "gradient vector flow snake" (GVF) [23,24]. Instead of directly using image gradients as an external force, it uses a spatial diffusion of the gradient of an edge map of the image. GVF snake was proposed to address the traditional snake's problems of short captured range and inability to track at boundary concavity. However, GVF still may not be able to capture object contours in some medical image segmentation. Efforts at improving the original GVF snake's performance have been published recently. Xu et al. combined GVF force with a constrained balloon force to segment gyri in the cortex [25]. Although this combination works well on this case, its requirement of an a priority knowledge of the region of interest may restrict its application.

In determinable success of defined ROIs, this paper proposes a new approach to enhance the GVF snake performance in kidneys segmentation on dynamic renal scintigraphy with ^{99m}Tc-DTPA and ^{99m}Tc-MAG3. The method consists of three major parts. Firstly, an adaptive elastic parameter has been developed to automatically adjust the rigidity of the snake during its evolution towards an image contour. Secondly, an adaptive balloon force is incorporated into internal forces to increase captured range and speed-up evolution. Thirdly, a dynamic GVF force is introduced to provide an evolution-stop mechanism. With this ability, the located contours are less sensitive to local minima. What is more, researcher evaluated the clinical applicability of the method for the estimation of GFR and ERPF by camera-based methods.

This paper is organized as follows. In Section 2, this paper presents methodology, which consists of materials and image acquisition, adaptive edge-based active contour models, camera-based methods, experiments and data analysis. Whereas, researchers detail adaptive edge-based active contour models in Section 2 for the mathematic foundation of active contour models, conventional snakes and GVF snakes, including different aspects of researcher's improved GVF snake using an adaptive elastic parameter, an adaptive ballon model and a dynamic GVF. In Section 3, this paper present some preliminary results of kidneys segmentation on dynamic renal scintigraphy and compare the performance of researchers' approach with the GVF snake. In addition, this paper evaluates the clinical applicability of the method for the estimation of GFR and ERPF by camera-based methods and compares the performance of the method with the APEX-XPERT program. Later, this paper presents discussion in Section 4. Finally, researchers propose conclusion and several avenues of research for future work in Section 5.

2. **Methodology.**

2.1. **Materials and image acquisition.**

There were four subjects (1 girl, 1 boy, 1 woman and 1 man) in age 6, 1, 58 and 34 years, respectively, included in the study. The subjects were referred for evaluation of renal function in routine nephrology practice. Informed consent was obtained prior to the test.

Gamma camera renography was performed on a dual head gamma camera (General Electric; Elscint-Varicam) with a low energy high-resolution collimator, and a 20% window

centred over the 140 keV photo peak of ^{99m}Tc. Patients remained supine on the bed above the gamma camera and were hydrated with a saline solution at 10 to 20 drops per minute during the exam. Following the intravenous injection of 3-5 mCi of ^{99m}Tc-DTPA or ^{99m}Tc-MAG3, the image data were collected in a 64×64 matrix at 2 seconds per frame in the initial 64 seconds and, thereafter, at 15 seconds per frame for 30 minutes. Gamma camera technique for GFR or ERPF calculation, a 1-minute image of the ^{99m}Tc-DTPA or ^{99m}Tc-MAG3 syringe before and after injection were taken 30 cm distance from center of the collimator. After injection, 15 seconds per frame images are acquired for a total of 6 minutes.

2.2. **Adaptive edge-based active contour models.** In this section, researchers review the mathematical formulation of conventional snakes and GVF snakes. Researchers also describe the strengths and weakness of each method.

In 2D, a snake is a curve $C(s) = (x(s), y(s))$ where $s \in [0, 1]$. The curve moves through the image domain to minimize a specified energy function. In traditional snakes, the energy is usually formed by internal forces and external forces as:

$$E_{snake} = E_{internal} + E_{external} \tag{1}$$

$E_{internal}$ tends to elastically hold the curve together (elasticity forces) and to keep it from bending too much (bending forces). This energy is defined in Equation (2), where $\frac{\partial C}{\partial s}$ and $\frac{\partial^2 C}{\partial s^2}$ represent the first and second derivative respectively. Researchers can control the snake's tension and rigidity by the coefficients α and β. $E_{external}$ intends to pull or push the curve towards the edges. Typically, the external forces consist of potential forces. This energy is defined in Equation (3), where E_{image} represents the negative gradient of a potential function. This energy is general the image force as defined in Equation (4) where I denotes the image and $X = X(x, y) = [x \ y]^t$. Using variational calculus and the Euler-Lagrange differential equation, researcher can solve Equation (1). Then, the solution of this force balance, as defined in Equation (5), represents the snake final position. The differences in the ways of the energy function is established and will result in different snakes.

$$E_{internal} = \frac{1}{2}\int_s \alpha \left|\frac{\partial C}{\partial s}\right|^2 ds + \frac{1}{2}\int_s \beta \left|\frac{\partial^2 C}{\partial s^2}\right|^2 ds \tag{2}$$

$$E_{external} = \int_s E_{image}(C(s))ds \tag{3}$$

$$E_{image}(X) = -|\nabla I(X)|^2 \tag{4}$$

$$\alpha\frac{\partial^2 C}{\partial s^2} - \beta\frac{\partial^4 C}{\partial s^4} - \nabla E_{image} = 0 \tag{5}$$

Although the traditional snakes have found many applications, they are intrinsical weak in three main aspects. First, they are very sensitive to parameters. Second, they have small captured range and the convergence of the algorithm is mostly dependent from the initial position. Finally, they have difficulties in progression into boundary concavities (Figure 2).

Xu and Prince have proposed a new GVF snake to achieve better object segmentation [24] and it is expressed as Figure 2. The basic idea of the GVF snake is to extend influence range of image force to a larger area by generating a GVF field. The GVF field is computed from the image. In detail, a GVF field is defined as a vector field $V = V(x)$ that minimizes the energy function.

$$Q = \iint \mu\nabla^2 V + |\nabla f|^2|V - \nabla f|^2 dx \tag{6}$$

where f is the edge map, which is derived by using an edge detector on the original image convoluted with a Gaussian kernel, and μ is a regularization parameter. Using variational calculus, the GVF field can be obtained by solving the corresponding Euler-Lagrange equations. Similar to Equation (5), the force balance equation of GVF snake can be expressed as

$$\alpha \frac{\partial^2 C}{\partial s^2} - \beta \frac{\partial^4 C}{\partial s^4} + \gamma V = 0 \tag{7}$$

where γ is a proportional coefficient. GVF snake's larger captured range and concavity tracking ability are attributed to the diffusion operation shown in the above equation. When $|\nabla f|$ is small, the energy is dominated by the sum of the squares of the partial derivatives of the vector field, resulting a slowly varying yet large coverage field. Whereas when $|\nabla f|$ is large, the second term dominates the integration.

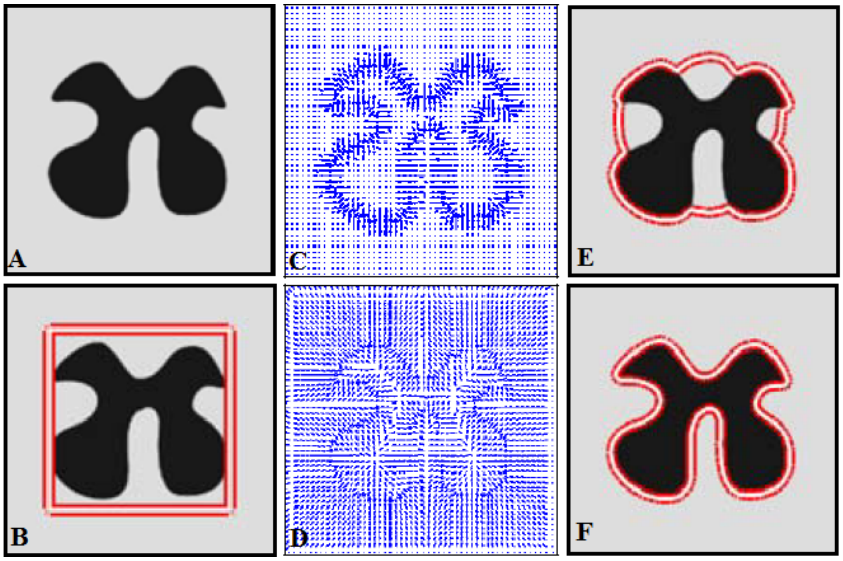

FIGURE 2. An object, its corresponding vectors and segmented results. (A) An object image. (B) The preliminary ROIs. (C) The corresponding vector by traditional active contour. (D) The corresponding vector by gradient vector flow. (E) Segmented result by traditional active contour. (F) Segmented esult by gradient vector flow.

In applying the GVF snake on real data such as medical images (Figure 3), the captured range of the active contour did not seem as large as researcher expected. This is mainly because in the case of medical data, images often contain a lot of textures. Unfortunately, the GVF field is very sensitive to these variations and the active contour does not converge to the ideal solution. Another observation was that the GVF snake was sensitive to the shape irregularities. In these cases, the GVF force could not properly push the snake to the right contour. To deal with these problems researchers have developed an improved GVF snake.

The improvement research proposal is to add new external forces, including an adaptive elastic parameter α, an adaptive balloon force $f_{adaptive\ pressure}$ and a dynamic GVF force, defined as a vector field $V_{dynamic}$. Then, researchers propose a new scheme to integrate these external forces in the snake mathematical formulation.

The adaptive elastic parameter has been developed to automatically adjust the rigidity of the snake during its evolution towards an image contour. Furthermore, the elasticity depends on time and the optimal preliminary ROIs cannot be specified beforehand. Thus, researchers propose an adaptive scheme, that automatically adjusts α parameter during

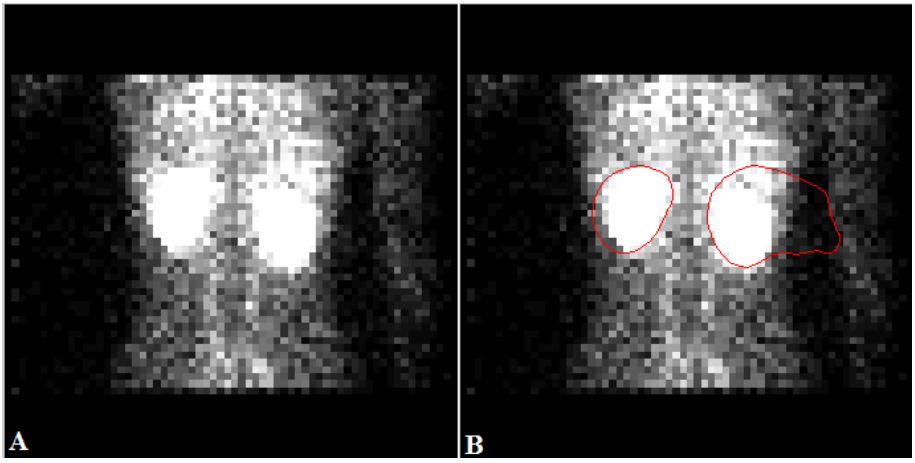

FIGURE 3. Automatic segmentation of kidney on gamma camera renography. (a) Original image. (b) Automatic segmentation by gradient vector flow.

its evolution towards an image contour. The α parameter based on a distance vector flow is defined by Equation (8).

$$\alpha = \frac{\omega}{1 + \mu \bar{D}_i} \tag{8}$$

where ω and μ are coefficients for controlling in the range of α values. $\bar{D}_i$ is the norm of $\vec{D}_i$ and normalized to have magnitude between 0 and 1. $\vec{D}_i$ is the candidate displacement. $\vec{D}_i$ is the difference between the snake's new position M_i and each point of snake N_i, that is attracted towards the nearest edge. In the part of edge, it is detected using the Canny operator. Thus, the new position M_i of point N_i is defined by Equation (9).

$$M_i = N_i + \vec{D}_i \tag{9}$$

In the balloon model proposed by Cohen et al., a pressure force $f_p(s)$ is added to snake force as a second external force to push the curve outward or inward [26,27]. In this way, the curve is considered as a balloon, that has been inflated or deflated. Equation (10) represents the pressure force, where $\vec{n}(s)$ is the normal unit vector to the curve at point $C(s)$.

$$f_p(s) = k \cdot \vec{n}(s) \tag{10}$$

The balloon force is considered to increase the captured range of image potential force. This is a proper consideration given, that the snake can be set to start evolving inside the object. Unfortunately, balloon force introduces unpredictability to the performance of the active contour and make it more sensitive to the value of its different parameters. To overcome the unpredictability problem introduced by the balloon force, this force is applied in an adaptive way. The main idea is to give the balloon force bigger weight compared to the GVF force at the early stage of the evolution, and to give the balloon force smaller weight at the later stage. In this way, the speed of the convergence is increased, and the snake can be correctly pushed towards the surface evenness if it starts far away with less chance of being over-pushed.

A dynamic GVF force is introduced to provide a unique evolution-stop mechanism as well as all the characteristics owned by the original GVF force. The evolution-stop mechanism is needed to prevent the snake from breaking through the correct contour and locking to other feature points. The breakage can happen in areas, where two objects or organs are very close to each other. The introduction of the dynamic GVF force is

inspired by a property of the GVF field. That is, when the GVF field passes a contour, its direction will change.

It can be easily observed that the field vector changes direction at the ellipse boundary. Therefore, a consistency degree is incorporated into the new dynamic GVF force. The force varies according to the consistency. If the evolution of the snake will cause the change of GVF force direction, it is said inconsistency has occurred and the snake is not allowed to evolve to the new position. With these three novel inclusions, the proposed force balance equation can be expressed as:

$$\alpha\frac{\partial^2 C}{\partial s^2} - \beta\frac{\partial^4 C}{\partial s^4} + \gamma V_{dynamic} + \lambda f_{adaptive\ pressure} = 0 \tag{11}$$

$V_{dynamic}$ is defined in Equation (12) as a dynamic gradient vector flow force. Let X_1 be a point on the current snake and X_2 be its possible next position in the evolution process. C_θ defines the consistency angle and is proportional to the angle between the GVF vectors at X_1 and X_2. To represent the cut-off angle, based on researcher's experiments, $T_\theta = 20°$ is a good threshold.

$$V_{dynamic} = \begin{cases} V & \text{if } C_\theta > T_\theta \\ \frac{-\alpha\frac{\partial^2 C}{\partial s^2} + \beta\frac{\partial^4 C}{\partial s^4} - \lambda f_{pa}}{\gamma} & \text{otherwise} \end{cases} \tag{12}$$

The new dynamic gradient vector flow force will be the same as conventional GVF if the snake point moves towards the contour. However, when the snake point tries to cross over an edge, the dynamic gradient vector flow force will stop the point from moving. The threshold T_θ will decide when this evolution-stop mechanism will be triggered.

2.3. **Camera-based methods.** After image acquisition, patient's weight and height were entered into an online computer, with which all imaging data were recorded. The GFR and ERPF were automatically calculated by a commercial available computer and the proposed method according to the Gate's algorithm and Schlegel's algorithm. GFR by modified Gate's method [28] was calculated with the following formula:

$$Total\ renal\ uptake\ percent\ (\%) = \frac{\left[\frac{(R-R_B)}{e^{-\mu D_R}} + \frac{(L-L_B)}{e^{-\mu D_L}}\right]}{(Pre - Post)} \tag{13}$$

$$Global\ GFR = Total\ percent\ renal\ uptake\ (\%) \times 100 \times 9.81270 - 6.82519 \tag{14}$$

where *Pre*: pre-count, *Post*: post-count, R: right kidney counts, R_B: right kidney background counts, L: left kidney counts, L_B: left kidney background counts, D_R: right kidney depth, D_L: left kidney depth, μ: attenuation coefficient of ^{99m}Tc in soft tissue (0.153/cm), e: constant.

The ERPF was calculated according to the protocol (method for ERPF analysis of Schlegel) based on the following:

$$ERPF = 5.029 \times Body\ Surface\ Area \times R \tag{15}$$

$$Body\ Surface\ Area = Weight(Kg)^{0.425} Height(cm) \times 0.007184 \tag{16}$$

and R is the predicted 32-minute return of the injected nuclide, defined as:

$$Predicted\ Return = \frac{Individual\ kidney\ uptake}{Total\ uptake\ and\ calculated\ on\ each\ side} \tag{17}$$

The *uptake* is calculated as follows:

$$Uptake = \frac{(Background\text{-}corrected\ counts)(Kidney\ Depth^2) \times 100}{One\text{-}minute\ counts} \tag{18}$$

From injection image, where

$$\begin{aligned} &Background\text{-}corrected\ counts \\ &= Raw\ Counts - \left(Background\ counts \times \frac{\#pixels\ in\ kidney\ ROI}{\#pixels\ in\ Background\ ROI} \right) \end{aligned} \tag{19}$$

Kidney depth was estimated from the correlations:

$$Right\ Kidney\ Depth = \frac{13.3 \times Weight(kg)}{Height(cm)} + 0.7 \tag{20}$$

$$Left\ Kidney\ Depth = \frac{13.2 \times Weight(kg)}{Height(cm)} + 0.7 \tag{21}$$

2.4. **Experiments and data analysis.** In validation for the performance of the proposed method, preliminary ROIs and background regions were manually drawn on the frame from summation of all frames in time 31 minutes and 4 seconds included, after the injection. Then, segmentations obtained by physicians and automated segmentations obtained by the method of GVF snake and the proposed method were performed for segmentation of kidneys. Kidneys and background regions were selected on images to obtain counts. The background corrected time-activity curve was generated and the renal uptake of individual kidneys for one minute from 2 to 3 minutes or 1-2 minutes after the injection was calculated for the estimation of GFR or ERPF, respectively. After correcting for background and attenuation, the net renal cortical uptake as a percentage of the total injected dose was calculated for the estimation of GFR and ERPF. The GFR and ERPF were automatically estimated by a commercially available computer programmer (APEX-XPERT program) and the proposed method according to the Gate's algorithm and Schlegel's algorithm, respectively.

Researcher's validation criteria of kidneys segmentation is based on both subjective and quantitative analysis. For subjective aspect, the contours drawn by experts and by automatic segmentation were compared. In addition, the quality of kidneys segmentation defined for each patient by the original GVF and the proposed method in the estimation of GFR 1 patient and all others ERPF was evaluated visually and graded as excellent, good, fair, or poor. The quality of kidneys segmentation was graded as excellent when the kidneys segmentation were concordant with renal areas identified visually, good when they were closely concordant with renal areas identified visually but showed some minor discrepancy, and fair when there was obvious discrepancy between the kidneys segmentation and renal areas identified visually but clinical use was considered permissible. When the generated kidneys segmentation were judged unacceptable for clinical use, their quality was graded as poor. The grading was independently done by nine physicians, who were unaware of the method of kidneys segmentation. In cases of discrepant assessments, the final decision was made by a tenth physician from taking account of the nine preceding assessments.

For quantitative analysis, three validating parameters are defined. Researchers have designed four experiments using four different sets of parameters for each patient in the estimation of GFR 1 patient and all other ERPF (Table 1). Researchers choose $\alpha = 0.1$ and $\lambda = 0.05$ for researcher's method. In defining the parameters, the accuracy of the snake results is checked against the manual segmentations done by three experts. To evaluate the results, researchers propose to use three values which researchers will denote by R_{CA}, F_{PN} and F_{NN}. R_{CA} is defined as the ratio between the area considered as kidney by both the snake and at least two experts and the area considered as kidney either by the snake or at least two experts. It is expressed as $R_{CA} = \frac{A_{overlap}}{\max(A_{expert}, A_{snake})}$, where

A_{snake} is the area confined by snake; A_{expert} is the area considered as kidney by at least two of the three experts and $A_{overlap}$ is the area overlapped between A_{snake} and A_{expert}. Researcher can note that R_{CA} is a normalized value ($R_{CA} \in [0, 1]$). F_{PN} is defined as the area considered as kidney by snake, but as non-kidney by at least two experts (False Positive Number). F_{NN} is defined as the area considered as non-kidney by snake, but as kidney by at least two experts (False Negative Number).

TABLE 1. Parameters set for the four experiments

Parameters / Patients	β	γ
Patient A for the GFR estimation	0.01	0.03
Patient B for the ERPF estimation	0.01	0.05
Patient C for the ERPF estimation	0.01	0.01
Patient D for the ERPF estimation	0.01	0.03

The estimation of GFR and ERPF were examined and compared between the proposed method and APEX -XPERT program using t test for accuracy evaluation. In most hypothesis-testing situations concerning the population mean, μ, researchers do not know the population standard deviation, σ. Instead, researchers use the sample standard deviation, S. If researchers assume that the population is normally distributed, the sampling distribution of the mean follows a t distribution with $n - 1$ degrees of freedom. If the population is not normally distributed, researcher can still use the t test if the sample size is large enough. Equation (22) defines the test statistic t for determining the difference between the sample mean, $\bar{X}$, and the population mean, μ, when the sample standard deviation, S, is used. The t test of hypothesis for the mean (σ unknown) is calculated with the following equation:

$$t = \frac{\bar{X} - \mu}{\frac{S}{\sqrt{n}}} \tag{22}$$

where the test statistic t follows a t distribution having $n - 1$ degrees of freedom.

3. **Main Results.** To investigate the performance of researcher's segmentation method and compare it with original GVF snake, both original GVF snake and researcher's improved GVF snake have the same values of β and γ, and researchers also set the initial position for the curve. Figure 4 shows the original image and the initial snake position drawn in red curve. Then, segmentations obtained by physicians and automated segmentations obtained by the method of GVF snake and the proposed method were performed for kidneys segmentation. For subjective aspect, the contours drawn by physicians and by automatic segmentation were compared. Figure 5 shows manual segmentation by experts. Figure 6 shows automatic segmentation using two different techniques with four sets of parameters for each patient. Figure 7 shows the (x, y) coordinates of kidneys from segmentations obtained by physicians and automated segmentations obtained by the method of GVF snake and the proposed method. Based on Figures 6 and 7, researcher can see that the original GVF can not correctly locate the kidneys and is stuck on unwanted features. Kidneys and background regions were selected on images to obtain counts and the counts were background subtracted to perform a camera-based GFR and ERPF calculation. Figure 8 shows kidneys and background regions were selected on images to obtain counts.

The results of visual evaluation for the quality of kidneys segmentation are presented in Table 2. For automatic segmentations obtain by researcher's improved snake, the quality

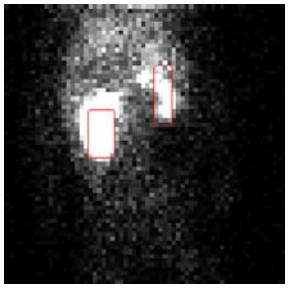

FIGURE 4. The original gamma camera renography slice 35 of fourth patients and the initial snake position drawn in red box

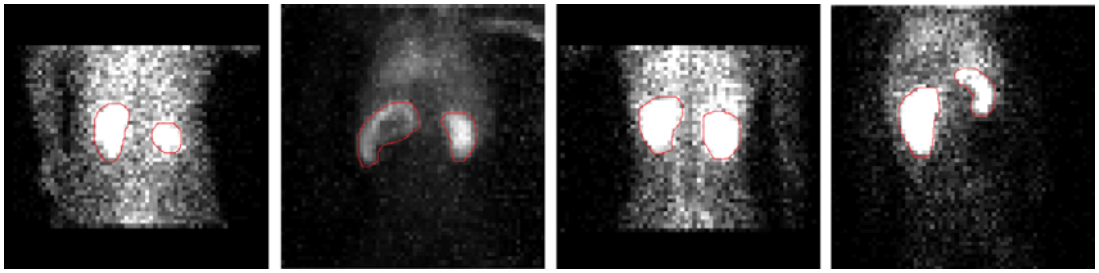

FIGURE 5. Manual segmentation by expert of kidneys on renal scintigraphy

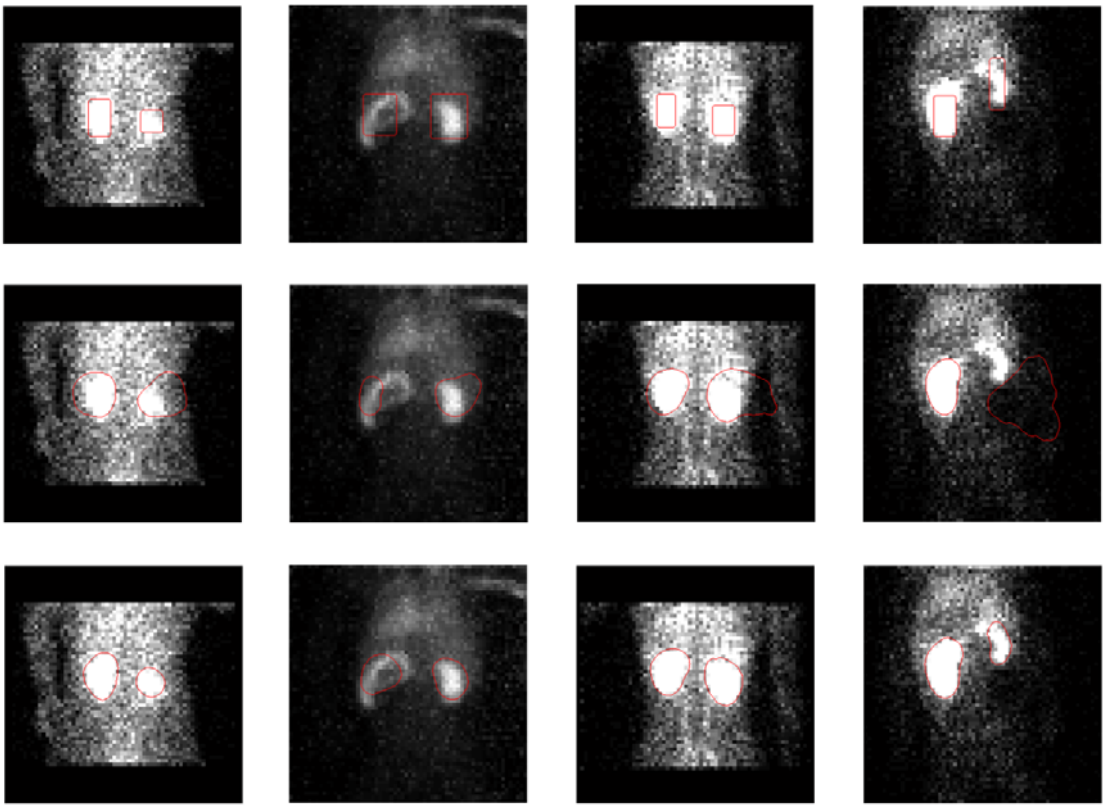

FIGURE 6. Kidneys segmentation on renal scintigraphy of four patients, using two different techniques. Top: the initial snake position; Middle: original GVF snake; Bottom: researcher's improved snake.

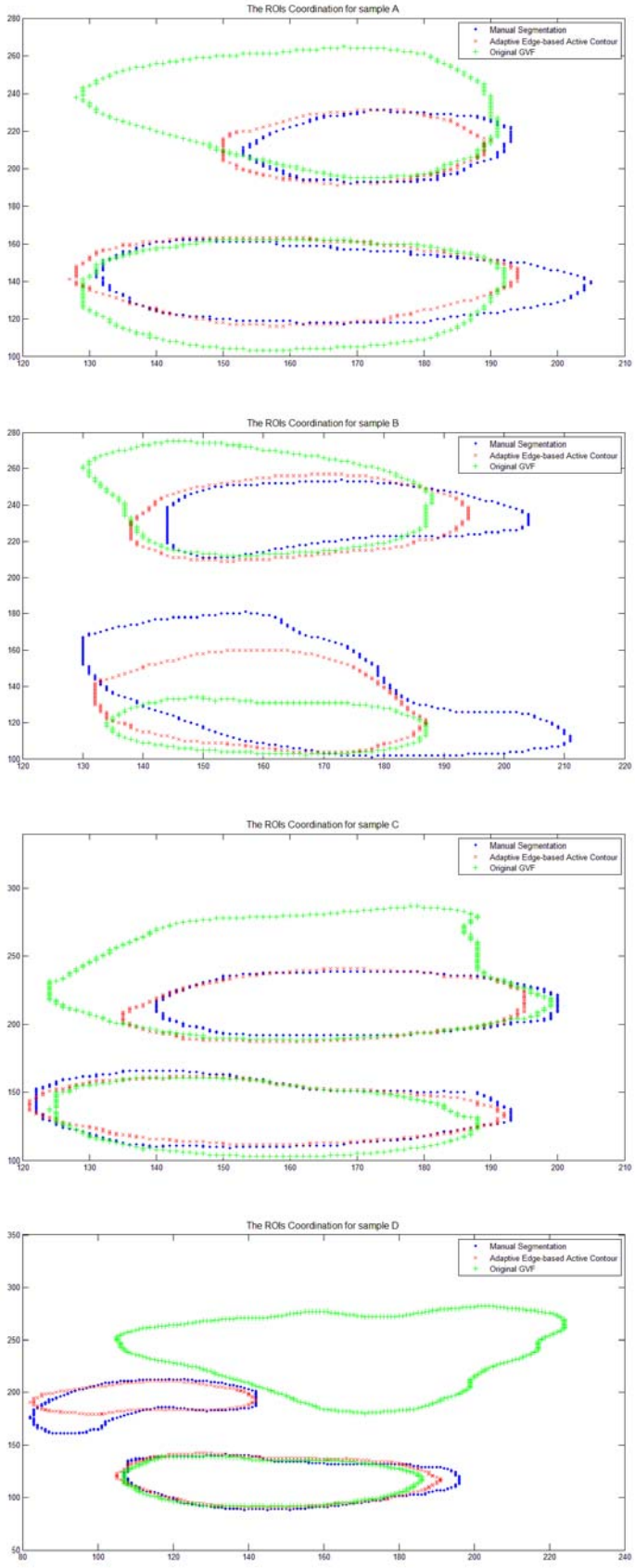

FIGURE 7. The (x, y) coordinates of kidneys from manual segmentations obtained by physicians and automatic segmentations obtained by the method of GVF snake and the proposed method.

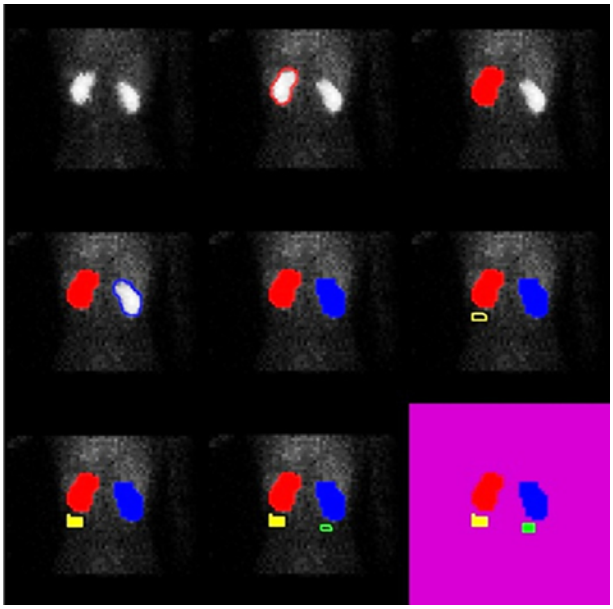

FIGURE 8. Kidneys and background regions were selected on images to obtain counts.

TABLE 2. Grading of quality of kidneys segmentation

Grade	The Proposed Method				Original GVF			
	A	B	C	D	A	B	C	D
Excellent	7	8	8	9	0	0	0	0
Good	2	1	2	1	0	0	0	0
Fair	1	1	0	0	4	2	3	0
Poor	0	0	0	0	6	8	7	10

TABLE 3. Values of three criteria using the original GVF snake and the improved GVF snake

Grade	Original GVF			The Proposed Method		
	R_{CA}	F_{PN}	F_{NN}	R_{CA}	F_{PN}	F_{NN}
Patient A for the GFR estimation	0.3931	835	63	0.9455	32	35
Patient B for the ERPF estimation	0.2127	529	1195	0.6983	89	393
Patient C for the ERPF estimation	0.2388	657	72	0.9274	16	22
Patient D for the ERPF estimation	0.0855	1237	39	0.8871	11	28

of kidneys segmentation with the measured GFR mean of 66.07 mL/min in sample A was graded as excellent in 7 physicians, good in 2 physicians, fair in 1 physician and poor in none. The quality of kidneys segmentation with the measured ERPF mean of 323.64 mL/min in sample B was graded as excellent in 8 physicians, good in 1 physician, fair in 1 physician and poor in none. The quality of kidneys segmentation with the measured ERPF mean of 233.34 mL/min in sample C was graded as excellent in 8 physicians, good in 2 physicians, fair and poor in none. The quality of kidneys segmentation with

the measured ERPF mean of 426.31 mL/min in sample D was graded as excellent in 9 physicians, good in 1 physician, fair and poor in none. For defined automatic segmentation obtained by original GVF snake, the quality of kidneys segmentation with the measured GFR mean of 66.07 mL/min in sample A was graded as excellent and good in none, fair in 4 physicians, and poor in 6 physicians. The quality of kidneys segmentation with the measured ERPF mean of 323.64 mL/min in sample B was graded as excellent and good in none, fair in 2 physicians and poor in 8 physicians. The quality of kidneys segmentation with the measured ERPF mean of 233.34 mL/min in sample C was graded as excellent and good in none, fair in 3 physicians and poor in 7 physicians. The quality of kidneys segmentation with the measured ERPF mean of 426.31 mL/min in sample D was graded as excellent, good and fair in none and poor in 10 physicians. Therefore, the proposed method provided kidneys acceptable for clinical use in all patients, including those with high and low renal function (Figure 6).

For quantitative analysis, the R_{CA}, F_{PN} and F_{NN} values of the original GVF snake and researcher's approach are presented in Table 3. Researcher can see that the original GVF snake gives R_{CA} unfavorable values of 0.3931, 0.4127, 0.2388 and 0.0855 comparing to 0.9455, 0.7983, 0.9274 and 0.8871, respectively, of researcher's approach. Subsequently, researcher can see that the original GVF snake gives F_{PN} values of 235, 229, 557 and 837 comparing to 2, 59, 6 and 3, respectively, of researcher's approach. And, the original GVF snake gives F_{NN} values of 63, 195, 72 and 59 comparing to 35, 93, 26 and 48, respectively, of researcher's approach. These do mean the area located by researcher's approach is more likely as kidneys than the area located by the original GVF snake. In addition, if researchers check the F_{PN} and F_{NN} values of researcher's method, that presented much less false positive number and false negative number. This is ideal from the viewpoint of a physician.

The estimation of GFR and ERPF with the proposed method is presented in Table 4. Researcher can see that the GFR and ERPF values by APEX-XPERT program gives values of 66.40, 322.80, 234.15 and 425.76 comparing to 66.07, 323.64, 233.34 and 426.31, respectively, of researcher's approach. For a given sample size, $n = 10$, researcher decide to use $\alpha = 0.05$ and the test statistic t follows a t distribution with $n - 1$ degrees of

TABLE 4. The mean of GFR and ERPF estimation using the proposed method

	GFR of Sample A	**ERPF of Sample B**	**ERPF of Sample C**	**ERPF of Sample D**
	64.74	324.87	232.58	426.72
	65.20	322.01	234.51	424.44
	68.53	321.98	230.36	428.66
	69.24	323.81	231.08	425.61
	63.61	325.35	235.66	427.67
	64.21	324.66	237.72	426.55
	66.61	321.64	234.67	428.41
	67.24	324.66	230.42	423.34
	63.11	325.77	233.62	424.61
	68.23	321.62	232.76	427.11
$\bar{X}$	66.07	323.64	233.34	426.31
μ	66.40	322.80	234.15	425.76
S	2.19	1.65	2.39	1.77

TABLE 5. Determining the critical value from the t table for an area of 0.025 in each tail with 9 degrees of freedom [29]

Degrees of Freedom	Upper-Tail Areas					
	.25	.10	.05	.025	.01	.005
1	1.0000	3.0777	6.3138	12.7062	31.8207	63.6574
2	0.8165	1.8856	2.9200	4.3027	6.9646	9.9248
3	0.7649	1.6377	2.3534	3.1824	4.5407	5.8409
4	0.7407	1.5332	2.1318	2.7764	3.7469	4.6041
5	0.7267	1.4759	2.0150	2.5706	3.3649	4.0322
6	0.7176	1.4398	1.9432	2.4469	3.1427	3.7074
7	0.7111	1.4149	1.8946	2.3646	2.9980	3.4995
8	0.7064	1.3968	1.8595	2.3060	2.8965	3.3554
9	0.7027	1.3830	1.8331	2.2622	2.8214	3.2498

freedom. The critical values of the t distribution with $10 - 1 = 9$ degrees of freedom are found in Table 5. The alternative hypothesis, H_1, $\mu \neq 66.40$, $\mu \neq 322.80$, $\mu \neq 234.15$ and $\mu \neq 425.76$ mL/min for GFR mean of sample A, ERPF mean of sample B, ERPF mean of sample C and ERPF mean of sample D, respectively, are two-tailed. Thus, the area in rejection region of the t distribution's left (lower) tail is 0.025, and the area in rejection region of the t distribution's right (upper) tail is also 0.025. From the t table shown in Table 5, the critical values are ± 2.2622. The decision rule is

$$\begin{array}{ll} \text{Reject } H_0 & \text{if } t < -t_9 = -2.2622 \\ \text{or} & \text{if } t > t_9 = 2.2622 \\ \text{otherwise,} & \text{do not reject } H_0 \end{array}$$

Because $-2.2622 < t = -0.4733 < 2.2622$ for GFR mean of sample A, $-2.2622 < t = 1.6017 < 2.2622$ for ERPF mean of sample B, $-2.2622 < t = -1.0764 < 2.2622$ for ERPF mean of sample C and $-2.2622 < t = 0.9836 < 2.2622$ for ERPF mean of sample D, researchers do not reject H_0. These do mean the mean of GFR and ERPF estimation using the proposed method successfully predicted from ten physicians for one patient evaluated GFR and all others evaluated ERPF.

4. **Discussion.** Based on the figures and tables, two main points can be drawn as to the performance comparison. One point is that, in terms of subjective criteria, the original GVF snake's captured range is far from enough to locate the kidneys and it easily became stuck on unwanted features and failed on most of the cases, whereas the proposed approach succeed in locating the kidneys in cases. Displaying kidneys segmentation on a dynamic renal scintigraphy is not essential for data processing, however, display aids in visually evaluation for the quality of kidneys segmentation. The proposed method defined kidneys acceptable on visual inspection in all patients, including those with GFR and ERPF estimation. The other point is that, according to quantitative analysis, researcher's approach resulted more preferable results than the original GVF snake. This does mean the area located by researcher's approach is more likely as kidney than the area located by the original GVF snake.

The GFR and ERPF were automatically estimated by a commercial available computer programmer (APEX-XPERT program) and the proposed method has insufficient evidence to conclude that the mean of estimated GFR and ERPF by the proposed method differs from the estimated GFR and ERPF by APEX-XPERT program because the null hypothesis cannot be rejected at the 5% level of significance. Therefore, the proposed

method presented in this paper can provide suitable kidneys for clinical use with limited operator intervention and appears to improve the feasibility of reliable estimation of GFR and ERPF.

However, only as small number of patients were examined in this study. Further validation should be done in patients with a variety of morphologies and differing function. To accurately estimate GFR and ERPF using the proposed method, the tightness of the definition of renal contour should be comparable with that in the institution, where the equations are developed. This is not warranted when ROIs are manually drawn, and the determination of the proposed equations may be required for each institution. Improved interinstitutional reproducibility is inferred to be a merit of reduced physician dependency. A multifarious trial appearance warrants to assess the accuracy and clinical usefulness of the camera-based method combined with the automatic kidneys segmentation.

5. **Conclusions.** In this paper, researchers have presented a new method using adaptive edge-based active contour models for kidneys segmentation on dynamic renal scintigraphy with ^{99m}Tc-DTPA and ^{99m}Tc-MAG3. Firstly, researcher presented an adaptive elastic parameter to automatically adjust the rigidity of the snake during its evolution towards an image contour. Secondly, researcher introduced an adaptive balloon force to increase GVF snake's capture range and speed up evolution. Finally, researcher proposed a dynamic GVF force to provide an efficient evolution-stop mechanism. Based on experiments on segmenting a kidney in renal scintigraphy data, it has shown that the proposed method is robust to the variation in initial position and efficient in preventing the snake from breaking through correct contour and locking to other feature points. The method defined visually acceptable ROIs with limited operator intervention and is suggested to be suitable for clinical use. The camera-based methods using the proposed method allowed estimation of GFR and ERPF with a high level of accuracy, do no differ from APEX-XPERT program at the 5% level of significance and negligible interoperator variability. Researcher's improved snake is expected to enhance the feasibility of reliable estimation of GFR and ERPF by a camera-based method. A current limitation of the method is that is independently deals slice by slice with 2D. As a consequence, researchers do not take into account the interslice spatial continuity of the gradient, or the possible anisotropy of the voxels and the principles discussed here apply to 3D.

Acknowledgment. This work is partially supported by Department of Telecommunications Engineering, King Mongkut's Institute of Technology Ladkrabang and Department of Industry Physics and Medical Instrument, King Mongkut's University of Technology North Bangkok. The authors also gratefully acknowledge the helpful comments and suggestions of the reviewers, which have improved the presentation.

REFERENCES

[1] K. Itoh, E. Tsukamoto, H. Kakizaki, K. Nonomura and M. Furudate, Comparative study of renal scintigraphy with ^{99m}Tc-mercaptoacetyltriglycine and ^{123}I-orthoiodohippurate, *Nucl. Med. Commun.*, vol.14, pp.644-652, 1993.

[2] A. Jr Taylor, P. L. Corrigan, J. Galt et al., Measuring technetium-99m-MAG3 clearance with an improved camera-based method, *J. Nucl. Med.*, vol.36, pp.1689-1695, 1995.

[3] K. Itoh, K. Nonomura, T. Yamashita et al., Quantification of renal function with a count-based gamma camera method using technetium-99m MAG3 in children, *J. Nucl. Med.*, vol.37, pp.71-75, 1996.

[4] A. Jr Taylor, A. Manatunga, K. Morton et al., Multicenter trial validation of a camera-based method to measure Tc-99m mercaptoacetyltriglycine, or Tc-99m MAG3, clearance, *Radiology*, vol.204, pp.47-54, 1997.

[5] M. S. Dagli, V. J. Caride, S. Carpenter and I. G. Zubal, Compartmental analysis of the complete dynamic scan data for scintigraphic determination of effective renal plasma flow, *J. Nucl. Med.*, vol.38, pp.1285-1290, 1997.

[6] N. Oriuchi, Y. Onishi, H. Kitamura et al., Noninvasive measurement of renal function with ^{99m}Tc-MAG3 gamma-camera renography based on the onecompartment model, *Clin. Nephrol.*, vol.50, pp.289-294, 1998.

[7] Y. Inoue, T. Ohtake, I. Yokoyama, K. Yoshikawa, S. Asai and K. Ohtomo, Evaluation of renal function from ^{99m}Tc-MAG3 renography without blood sampling, *J. Nucl. Med.*, vol.40, pp.793-798, 1999.

[8] P. C. Jackson, M. Jones, C. E. Brimble and J. Hart, The reduction of inter- and intra-observer variability for defining regions of interest in nuclear medicine, *Eur. J. Nucl. Med.*, vol.11, pp.186-189, 1985.

[9] R. K. Halkar, Y. Chrem, J. R. Galt et al., Interoperator variability in quantitating the MAG3 renal uptake based on semiautomated and manual regions of interest, *J. Nucl. Med.*, vol.37, no.293, 1996.

[10] Y. Tomaru, T. Inoue, N. Oriuchi, K. Takahashi and K. Endo, Semiautomated renal regions of interest selection method using the double-threshold technique: Inter-operator variability in quantitating ^{99m}Tc-MAG3 renal uptake, *Eur. J. Nucl. Med.*, vol.25, pp.55-59, 1998.

[11] D. R. R. White, A. S. Houston, W. F. D. Sampson and G. P. Wilkins, Intra- and interoperator variations in region-of-interest drawing and their effect on the measurement of glomerular filtration rates, *Clin. Nucl. Med.*, vol.24, pp.177-181, 1999.

[12] M. F. Lythgoe, I. Gordon, Z. Khader, T. Smith and P. J. Anderson, Assessment of various parameters in the estimation of differential renal function using technetium-99m mercaptoacetyltriglycine, *Eur. J. Nucl. Med.*, vol.26, pp.155-162, 1999.

[13] M. Yamashita, H. Yamagishi, M. Hashiba, M. Nakata, M. Fujita and H. Nakahashi, Atrial of automatic kidney detection in a dynamic renal study, *Radioisotopes*, vol.36, pp.590-593, 1987.

[14] P. Hannequin, J. C. Liehn and J. Valeyre, Cluster analysis for automatic image segmentation in dynamic scintigraphies, *Nucl. Med. Commun.*, vol.11, pp.383-393, 1990.

[15] A. S. Houston, D. R. R. White, W. F. D. Sampson, M. A. Macleod and J. B. Pilkington, An assessment of two methods for generating automatic regions of interest, *Nucl. Med. Commun.*, no.19, pp.1005-1016, 1998.

[16] M. Samal, C. C. Nimmon, K. E. Britton and H. Bergmann, Relative renal uptake and transit time measurements using functional factor images and fuzzy regions of interest, *Eur. J. Nucl. Med.*, vol.25, pp.48-54, 1998.

[17] A. Jain, Y. Zhong and M. Dubuisson-Jolly, Deformable template models: A review, *Signal Processing*, vol.71, pp.109-129, 1998.

[18] T. McInerney and D. Terzopoulos, A dynamic finite element surface model for segmentation and tracking in multidimensional medical images with applications to cardiac 4D image analysis, *Computerized Medical Imaging and Graphics*, vol.19, no.1, pp.69-83, 1995.

[19] C. Xu and J. Prince, Generalized gradient vector flow external forces for active contours, *Signal Processing*, vol.71, pp.131-139, 1998.

[20] M. Kass, M. Witkin and D. Terzopoulos, Snakes: Active contour models, *International Journal of Vision*, vol.1, pp.321-331, 1987.

[21] T. McInerney and D. Terzopoulos, Deformable models in medical image analysis: A survey, *Medical Image Analysis*, vol.1, no.2, pp.91-108, 1996.

[22] P. Bamford and B. Lovell, Unsupervised cell nucleus segmentation with active contours, *Signal Processing Special Issue: Deformable Models and Techniques for Image and Signal Processing*, vol.71, no.2, pp.203-213, 1998.

[23] C. Xu and J. Prince, Generalized gradient vector flow external forces for active contours, *Signal Processing*, vol.71, pp.131-139, 1998.

[24] C. Xu and J. Prince, Snakes, shapes, and gradient vector flow, *IEEE Transactions on Images Processing*, vol.7, no.3, pp.359-369, 1998.

[25] C. Xu, D. Pham, M. Rettmann, D. Yu and J. Prince, Reconstruction of the human cerebral cortex from magnetic resonance images, *IEEE Transactions on Medical Imaging*, vol.18, no.6, pp.467-479, 1999.

[26] L. Cohen, On active contour models and balloons, *Computer Vision, Graphics, and Image Processing: Image Understanding*, vol.53, no.2, pp.211-218, 1989.

[27] L. Cohen and I. Cohen, Finite-element methods for active contour models and balloons for 2-d and 3-d images, *IEEE Transactions on Pattern Analysis and Machine Intelligence*, vol.15, no.11, pp.1146-1131, 1993.

[28] G. F. Gates, Split renal function testing using Tc-99m DTPA, A rapid technique for determining differential glomerular filtration, *Clin. Nucl. Med.*, vol.8, pp.400-407, 1983.

[29] D. M. Levine, D. F. Stephan, T. C. Krehbiel and M. L. Berenson, *Statistics for Managers Using Microsoft Excel*, 5th Edition, Prentice Hall Upper Saddle River, New Jersey, 2008.